

Unconstrained dynamic gel swelling generates transient surface deformations

Alyssa VanZanten¹, Shih-Yuan Chen², Michelle M. Driscoll², and Caroline R. Szczepanski¹

¹Department of Chemical Engineering and Materials Science, Michigan State University

²Department of Physics and Astronomy, Northwestern University

June 24, 2024

Abstract

Polymer gels are comprised of a three-dimensional, cross-linked network that can typically withstand the mechanical deformation associated with both swelling and de-swelling. Thus, gels can be designed with smart behaviors that require both stress generation and dissipation, making them well-suited to many applications including membrane technology, water capture devices, and drug delivery systems. In contrast to the fully swelled equilibrium state, limited research characterizes the unsteady-state swelling regime prior to equilibrium. It is in this regime where unique surface deformations can occur. Here we show how internal network constraints and external diffusive pressure can be leveraged to manipulate swelling kinetics and surface deformations in poly(ethylene glycol) gels during unconstrained, three-dimensional swelling. We find that increasing cross-linker molecular weight and swelling in ethanol, as opposed to water, are both effective routes to increase the time it takes to reach equilibrium but do so through different mechanisms. Networks with fewer internal constraints, manipulated via cross-linker chain-length, imbibe more solvent over a longer time. In contrast, swelling in ethanol reduces the amount of solvent imbibed by the network while increasing the time to reach equilibrium. Measurements of surface patterns during swelling establishes that an immediate, fast relaxation at the surface occurs during the first five minutes of swelling. However, the density and persistence of these features varies with solvent quality. These results serve to establish a framework for how soft materials undergo dynamic deformation. Engineering transient surface properties while mitigating unwanted instabilities opens the door for emerging technologies such as smart anti-fouling and sensors.

1 Introduction

The development of smart soft materials in recent years has largely focused on utilizing stimuli-responsive polymers, because of the numerous synthetic pathways available to tailor their responsive behavior [1–4]. For example, hydrogels, which are cross-linked, elastic polymer networks capable of absorbing large amounts of liquid, can be designed to swell and de-swell in response to external stimuli, like heat, solvent quality, and light [5,6]. These qualities make hydrogels attractive for targeted drug delivery systems [7,8] and tissue engineering [9,10]. For instance, controlled release in delivery applications requires precise tailoring of transport kinetics [11] and internal forces [12], such as the generation and dissipation of stresses during gel swelling. Interestingly, the significant internal stresses that arise during swelling are known to induce instabilities, such as bulk buckling and surface deformation [13–15]. These instabilities are relevant and must be understood at a fundamental level, since changes at the surface of a material can dramatically impact its interactions with surrounding fluids. Thus, establishing how synthetic handles, such as cross-link density, impact surface deformation is critical when tailoring gels for specific application fields. This work utilizes hydrogel swelling as a platform to establish the fundamental stress generation and dissipation mechanics that lead to reversible surface deformation in soft materials.

To understand swelling of a polymer network at a fundamental level, researchers often turn to Flory-Rehner polymer solution theory, which posits that gel swelling is driven by two opposing forces: (1) the force of mixing that results from the attraction between the polymer network and the solvent, and (2) the opposing elastic force that is due to the resistance of the elastic network to stretching during swelling [16–18]. This theory successfully summarizes the complex interplay of forces that govern swelling, and therefore captures a broad range of gel swelling phenomena, such as the existence of continuous and discontinuous volume phase changes, and the effects of temperature, pH, and salt concentration on swelling [19]. However, while Flory-Rehner describes the fully swelled, equilibrium state, there are systems to which this theory cannot be applied. For example, the use of macromeric (e.g., longer) cross-

linkers, which are common in hydrogel development, deviates from the small-chain cross-links proposed by Flory-Rehner [20,21]. Furthermore, Flory-Rehner assumes that a polymer network is in an equilibrium state (i.e., that the chemical potential (μ) is equivalent inside and outside of the gel); When considering the unsteady-state swelling regime prior to equilibrium, this assumption no longer holds true. Thus, understanding transient swelling behavior prior to an equilibrium state remains a challenge. Bulk instabilities such as spontaneous fracture and dynamic surface deformation arise during non-equilibrium swelling, which highlights the need to understand this transient behavior [13,22]. Understanding the origin of these instabilities will provide information on how localized stress gradients arise during swelling, as well as the mechanisms by which mismatched internal stresses are dissipated during transient swelling.

Despite the limited characterization of transient swelling, prior studies on equilibrium systems provide guidance as to what parameters can significantly impact gel swelling. For instance, we know that equilibrium swelling depends on cross-linking [23], polymer-solvent interaction [24], and environmental conditions [18,25]. Additionally, studies that analyze the kinetics of swelling show that geometry [26], polymer-solvent interaction [27,28], and diffusion rate [29] strongly impact swelling, but more work is needed to understand how these factors influence the dynamics of internal stress during the entire swelling process. Building upon this foundation, here we examine the changes in transient swelling and instability behaviors (e.g. surface deformations such as wrinkling, creasing, and folding) due to variations in both network constraints and solvent quality.

Many models of hydrogel swelling have been developed to capture these instability behaviors, which are driven both by solvent diffusion and non-linear, viscoelastic deformation of the polymer network [27,30–35]. However, these models typically assume a two-dimensional material geometry consisting of a thin ‘skin’ layer adhered to a softer foundation. With this geometry, the wavelength and amplitude of wrinkles on the surface are related to the compressive force in the skin layer [36]. Furthermore, in many two-dimensional systems, sur-

face deformations are engineered by imposing bulk strain, either manually through stretching [37,37,38] or by constraining a gel to a substrate during swelling [12,15,37,39,40,40–43], as well as by creating a depth-wise cross-linking gradient [15,44–46]. While these models and prior works characterize and describe behaviors such as wrinkling in coatings and thin films, assumptions that the elastic modulus and skin layer thickness are at steady-state do not apply to the system presented herein, which features free, unconstrained gel swelling, where material parameters are transient. While characterizing surface deformations in a transient, unconstrained system is challenging, it is crucial for engineering applications as these instabilities can be leveraged to impart anti-fouling or adhesive properties [36,47].

To describe the network response during swelling, we can consider three aspects that evolve dynamically and are inter-related: (1) swelling kinetics, (2) stress dynamics, and (3) surface deformation mechanics. *Swelling kinetics* defines the rate at which solvent is transported into and through a gel, and is dependent on many factors, such as cross-link density and polymer-solvent attraction [11,26,29,46,48]. Swelling kinetics depend on how effectively polymer chains can move and stretch in response to swelling, as well as diffusion of solvent molecules. When swelling begins, the surface of a gel becomes saturated and stretches to accommodate diffusing solvent while being constrained by the inner portion of the material that is not yet expanding or responding to swelling, since the solvent molecules have not yet diffused to the interior. These kinetics broadly influence *stress dynamics*, such as the stress that builds up due to mismatched swelling in the outer versus inner regions and the compressive stress experienced at the surface of the gel [7]. The magnitude of stress experienced locally changes based on the speed at which the saturated outer region diffuses inwards toward the unsaturated center. As a result of internal stress changing and dissipating, *surface deformation* is observed to be transient as swelling progresses. The solvent-saturated outer layer becomes softer than the bulk [17,43], and this mismatch between layers results in a buildup of compressive stress at the surface, thus leading to deformation (e.g., creasing) [14,39,40,49]. The evolution of surface instabilities is directly linked to swelling kinetics,

stress dynamics, and therefore network relaxation. Measurements of how creasing patterns evolve during swelling can give us a window into the mechanics of dynamic deformation.

The work presented here utilizes a three-dimensional bulk swelling setup, where the samples are not constrained during swelling and therefore imbibe water on all faces. We present unique, transient creasing of poly(ethylene glycol)-based gels and characterize both the swelling kinetics and surface deformation evolution. In Section 3.1 we characterize the instability behaviors that occur during transient swelling, focusing on the three-stages of surface deformation. We highlight a grid-like surface pattern that emerges after 20 minutes of swelling, which has only been described in a limited context prior to this work [13]. The impact of network constraints on swelling kinetics and capacity is investigated in Section 3.2 by manipulating cross-link fraction and molecular weight of the cross-linker employed. We also characterize how external diffusive pressure can be modulated via (co)solvent quality in Section 3.3. Specifically, swelling in ethanol as opposed to water is shown to decrease the rate of solvent imbibement, while the rate of swelling in water-ethanol (co)solvents changes non-monotonically with respect to ethanol content. Finally, crease evolution and kinetics are quantified through imaging measurements to infer stress dynamics in Section 3.4. This study will be used to understand the fundamental factors, both internal and external, that drive network relaxation during swelling.

2 Experimental Section

2.1 Materials

The base monomer employed in this study is poly(ethylene glycol) methyl ether acrylate (PEGMA) with a molecular weight of 400 g/mol. To form a network structure (gel), a cross-linker was incorporated into the polymerization. Two different poly(ethylene glycol) diacrylate (PEGDA) cross-linkers were employed, one with an average molecular weight of 700, and the other 10,000 g/mol. In all formulations, the photoinitiator used was 2,2-dimethoxy-2-phenylacetophenone (DMPA). All materials were obtained from Sigma-Aldrich and were used as received. For swelling experiments, deionized (DI) water was obtained via an in-house DI water source and 200-proof ethanol was obtained from Koptec. (Co)solvent solutions were prepared by mixing DI water and 200-proof ethanol at the following volume ratios: 90:10, 75:25, 50:50, 25:75, and 10:90 (water:ethanol).

2.2 Methods

Formulation Preparation and UV Curing

To manipulate network structure, two different control parameters were employed when formulating resins: (1) the relative fraction of cross-linker (PEGDA) and (2) the molecular weight of cross-linker employed (PEGDA-700 or PEGDA-10,000), as shown in **Table 1**. Throughout the remainder of the manuscript, formulations will be referenced by their name, which follows the pattern PEGDA(mol%):PEGMA(mol%). If the formulation was made with PEGDA-10,000, it is noted by the use of “10k” at the beginning of the name. If this notation is absent, PEGDA-700 was used in the formulation.

Table 1: Hydrogel formulations and naming scheme. The hydrogel formulations explored in this study were prepared with different loadings and molecular weights of cross-linker. Rows highlighted pink indicate formulations that typically exhibit surface deformation during transient swelling, and rows highlighted light gray do not exhibit surface deformation but are likely to spontaneously fracture during swelling.

Name	700 Mn	
	PEGDA (mol%)	PEGMA (mol%)
1:99	1	99
5:95	5	95
10:90	10	90
20:80	20	80
40:60	40	60
Name	10,000 Mn	
	PEGDA (mol%)	PEGMA (mol%)
10k 1:99	1	99
10k 10:90	10	90
10k 20:80	20	80
10k 40:60	40	60

The photoinitiator loading in all formulations was 0.5 wt%, meaning that the loadings listed for PEGMA and PEGDA in **Table 1** constitute 99.5 wt% of the total mass. Resins made with the 700 g/mol PEGDA were prepared neat (i.e., without solvent). In brief, the appropriate mass of DMPA, PEGMA, and PEGDA-700 were incorporated into a glass vial and magnetically stirred until homogeneous (~ 15 mins). To achieve a homogeneous resin formulation when employing the high molecular weight cross-linker (PEGDA-10K), water was included in the resin. This was incorporated to homogenize all resin constituents during mixing. After achieving a homogeneous mixture, the resin was dried at 65°C overnight, resulting in at least 95% of the water being removed as evidenced by the mass change after drying.

All polymerized samples were prepared in glass molds with approximate dimensions of 25 x 10 x 2 mm ($l \times w \times t$). Samples were photocured at an intensity of $0.1 \frac{W}{cm^2}$ in the UV-A region ($\lambda \sim 315$ to 400 nm). UV irradiation intensity was verified with a UV radiometer (Power Puck II, Electronic Instrumentation and Technology, Inc.).

Swelling Investigations

To measure swelling ratio (Q , **Eq. 1**), the mass of the as-prepared, dry, unswollen gel (m_0) was recorded prior to the gel being submerged in a large excess (approximately 50 mL) of solvent (deionized water, 200-proof ethanol, or a mixture of both). The gel was then removed from the solvent at predetermined swelling times. Upon removal, residual solvent was gently dabbed off the sample with a kimwipe, and the mass of the gel ($m(t)$) was recorded. The gel was then placed back into the solvent to continue swelling. This process was repeated over 24 hours of swelling to capture the entire range of behavior, including the equilibrium mass of the gel (m_{eq}). For samples that catastrophically ruptured during swelling, all pieces were removed from the solvent, dried, and weighed at each subsequent predetermined swelling time.

$$Q(t) = \frac{m(t)}{m_0}, \quad Q_{eq} = \frac{m_{eq}}{m_0}, \quad Q_0 = \frac{m_0}{m_0} = 1 \quad (1)$$

Swelling data was collected in triplicate for every formulation (**Table 1**) and solvent condition. The average and standard deviation of the swelling ratio at each time point (t) were used to calculate $\overline{Q(t)}$, the normalized swelling ratio (**Eq. 2**) and its associated error.

$$\overline{Q(t)} = \frac{m(t) - m_0}{m_{eq} - m_0} = \frac{Q(t) - Q_0}{Q_{eq} - Q_0} = \frac{Q(t) - 1}{Q_{eq} - 1} \quad (2)$$

In this equation, the relative swelling ratio increase at time (t) is divided by the total relative swelling ratio increase at equilibrium. Therefore, the normalized swelling ratio ($\overline{Q(t)}$) represents the fraction of the total swelling capacity that is reached at each time point.

Lastly, initial swelling kinetics were characterized via the swelling rate (e.g., Q as a function of time) during the first 30 minutes of solvent exposure in order to describe the entire range of swelling during which surface deformation (i.e., creasing) is observed. To obtain this rate, a linear equation was fit to the Q data during the first 30 minutes of swelling. The y-intercept of the linear fit was fixed at 1 as $Q_0 = 1$ (see, **Eqn. 1**). These initial swelling rate calculations are shown in **Fig. S1**.

Hydrogel Morphology Observations and Measurements

To visualize macroscopic surface deformation during swelling experiments, gel samples were removed, blotted dry, and photographed via iPhone XR. For smaller scale, frequent imaging, *in situ*, optical microscopy (Olympus Microscope ix83) was employed. 1:99, PEGDA-700 samples were swelled while microscope images (with a field of view of $6656 \mu\text{m} \times 6656 \mu\text{m}$) were captured every 20 seconds during the first 31.6 minutes of swelling. To ensure that there was no contact with the surrounding vessel inhibiting diffusion, each hydrogel sample was suspended off the bottom of the dish during swelling. The plane of focus of the microscope was aligned with the bottom of the sample, meaning that creases on the bottom appeared as thin, dark lines, whereas the out-of-focus creases on the top surface show up as larger, dark splotches. See **Figs. S3 - S4** for a clear depiction of the surface features we measured, in which the crease tracings in orange are overlaid on the microscope images.

To extract quantitative data from these microscope images, the crease lines were manually traced using MS Paint on a Microsoft Surface tablet. This process binarizes the images and provides accurate locations for the crease lines. Using a custom Python code, the geometric mean point of each line was identified from the images. Then, the closest neighboring point was identified, any duplicate reported distances were eliminated, and the average distance between neighboring creases was calculated. Once an ensemble of the distance between each crease line was established, the ensemble was averaged to obtain the characteristic “wavelength” or distance between observed crease patterns. Three samples were imaged for each solvent mixture. Given the complexity associated with the tracing process, seven equally spaced time points (20, 320, 640, 940, 1300, 1600, and 1900 seconds) were chosen for analysis to capture the range of instability behaviors.

3 Results and Discussion

3.1 Instability Behaviors During Transient Swelling

Qualitative observation of swelling behavior for each gel formulation (**Table 1**) reveals two types of instabilities during transient solvent diffusion; complex surface deformation (e.g., **Fig. 1a-h**) and catastrophic rupture (e.g., **Fig. 1i,j**). Surface deformations were observed for six formulations during swelling in water: 1:99, 5:95, and all formulations employing the 10k cross-linker (pink entries, **Table 1**). The remaining formulations (10:90, 20:80, and 40:60, gray entries, **Table 1**) did not exhibit macroscopic surface deformations during swelling in water, but often exhibited self-rupture. All samples that underwent surface deformation during transient swelling exhibited the same three-stage surface feature evolution: **creasing**, **grid**, and **equilibrium**. Immediately after being placed in an excess of solvent (e.g., on the order of seconds), small **creases** (detectable with the naked eye) appeared (see **Fig. 1b**). As swelling progressed (e.g., over many minutes), these surface features grew and coalesced, and additional self-contact occurred between “cells” as seen in **Fig. 1c,d**. As swelling continued, a long-range **grid** pattern emerged (see **Fig. 1e,f**, and **g**). At later swelling stages (e.g. 70 minutes of swelling or longer), the grid was still visible, although it became less distinct. Finally, the surface of the gel became smooth again (**Fig. 1h**) once the gel reached its final, **equilibrium** state. Equilibrium swelling is verified by constant $Q(t)$ values (e.g., plateauing to Q_{eq}).

Prior experimental work describes related surface deformations, such as creasing in gels that are attached to a substrate [15, 39, 41, 42] or under constraint [50, 51], as well as bulk buckling in gels with an engineered gradient in cross-link density [44, 46] or layered structure [49, 52]. However, to the best of our knowledge, the observed “**grid**” surface patterning during swelling has only been seen in one previous study, which found that this instability pattern was coupled to bulk buckling of hydrogel discs [13]. The similar, anisotropic grid-like crease pattern in our system provides perspective on how other sources of anisotropic

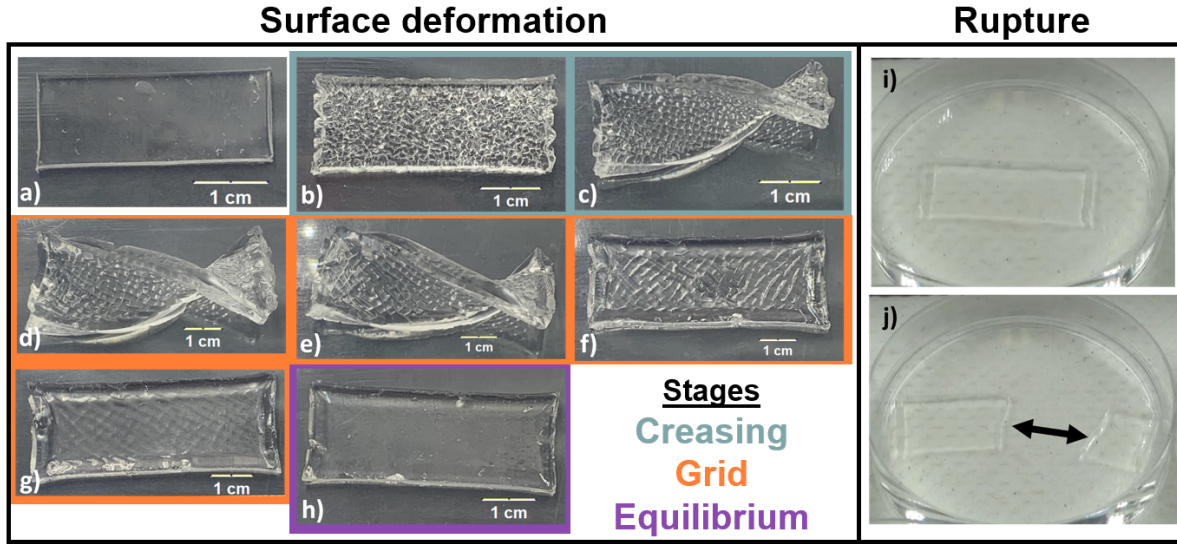


Figure 1: Examples of instability behaviors during swelling in water. First, the evolution of surface deformation for a 1:99, PEGDA-700 sample is shown at various swelling times, and the stages of instability are categorized as follows: a) 0 min before swelling begins, then **creasing** begins from b) 5 min, c) 10 min, then d) the **grid** pattern emerged at 20 min, e) 30 min, f) 50 min, g) 70 min, and h) the surface became smooth by 168 min, indicating **equilibrium**. Second, i) a 10:90, PEGDA-700 sample is shown at the start of swelling, and j) spontaneous rupture was observed after 14 minutes of swelling.

internal stresses can be engineered. Self-rupture behavior is addressed in computational studies on constrained swelling leading to fracture [31], and in experimental studies where rupture occurred during free swelling [22], as well as pre-programmed rupture induced by non-uniform swelling [53]. Theory has been developed to understand how stress due to swelling contributes to surface deformation in free-swelling spheres [32] and in constrained gel blankets [43], and how in soft materials internal stresses are often dissipated through instabilities (e.g. creases, wrinkles, or buckling). Here, we explore how surface deformations are coupled to both material properties (network architecture) and swelling kinetics (solvent selection) in a free-swelling gel, where no mechanical constraints are applied during the swelling process. Understanding the coupling between these swelling control parameters in an unconstrained system is necessary to design and tailor structured and dynamic material interfaces.

3.2 Impact of Internal Network Constraints

All samples containing the high MW cross-linker (PEGDA-10,000, denoted by “10k” in our sample notation) exhibited surface creasing and deformation during swelling in water; no rupture events were observed regardless of cross-linker fraction (mol%). This is in contrast to formulations containing the lower molecular weight cross-linker (PEGDA-700), where high cross-linker content (10 mol% or greater) corresponds to a high likelihood of rupture and no observable surface creasing or deformation. This indicates that internal network constraints significantly impact swelling kinetics and solvent diffusion. To quantify this behavior, we measure the swelling ratio $Q(t)$ (**Eq. 1**, **Fig. S1**); we report swelling for all samples as the normalized swelling ratio \overline{Q} , which is 0 in a dry gel and 1 for a fully swollen (equilibrium) gel (**Fig. 2a,b**). At each time point, \overline{Q} indicates the fraction of the total swelling capacity the gel has obtained. Higher \overline{Q} at earlier times indicate samples that quickly reach a high fraction of equilibrium swelling ratio (Q_{eq}), which is often a result of the total swelling capacity being relatively small (e.g., Q_{eq} for the 40:60 gels is 1.88, whereas for 1:99 gels this value is 6.75 - **Fig. 2d**). Thus only a small amount of water is imbibed to reach a high \overline{Q} .

The influence of cross-linker MW can be understood by comparing the \overline{Q} data for PEGDA-700 formulations (**Fig. 2a**) with PEGDA-10,000 formulations (**Fig. 2b**). Overall, we find that \overline{Q} is higher at early times for the PEGDA-700 samples. While most formulations with the PEGDA-700 cross-linker reach equilibrium relatively quickly, the 1:99 formulation takes a much longer time. Similar behavior is observed if the cross-linker MW is increased (10K - **Fig. 2b**). Gels with 1 mol% of the higher MW cross-linker (10k 1:99) are slower to achieve equilibrium, and increasing cross-linker fraction generally decreases the time to equilibrium.

To quantify the differences in time to equilibrium across various network architectures, each \overline{Q} dataset was fit with the following equation:

$$\overline{Q} = 1 - \exp\left(\frac{-t}{\tau}\right) \quad (3)$$

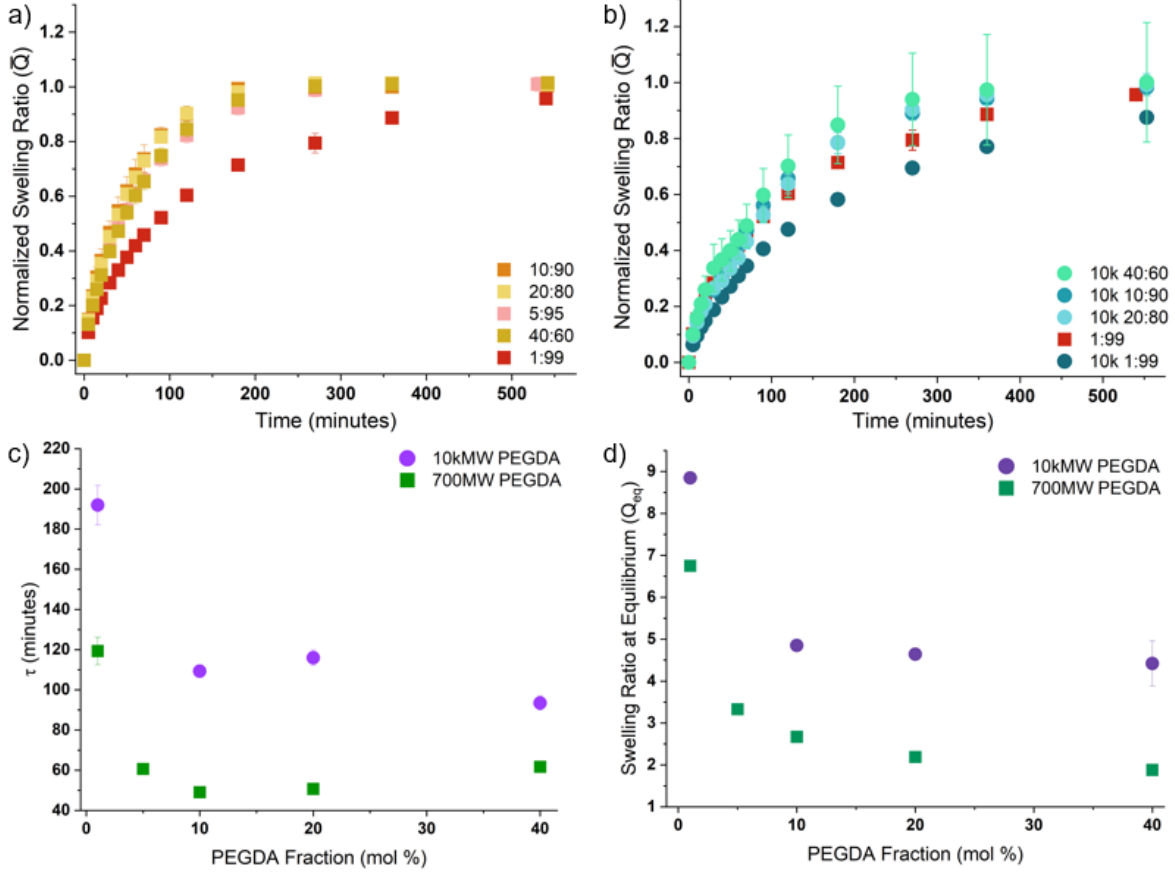


Figure 2: Tuning internal network constraints leads to measurable differences in swelling behavior (i.e. normalized swelling ratio (\bar{Q}), time to equilibrium (τ), and equilibrium swelling ratio (Q_{eq})). a) Normalized swelling ratio (\bar{Q}) vs. time, which represents the fraction of the total swelling capacity for gel formulations containing the 700MW PEGDA cross-linker. b) Normalized swelling ratio (\bar{Q}) vs. time for gel formulations utilizing the 10,000MW PEGDA cross-linker. Here the 1:99 formulation with the 700MW cross-linker is also plotted for reference. c) τ , the characteristic time parameter for \bar{Q} (Eq. 3), is plotted versus the fraction of cross-linker (PEGDA) in all gel formulations. An example fitting to obtain τ is provided in Fig. S2. Generally, these data show that a decrease in cross-linker fraction corresponds to a decrease in \bar{Q} at early swelling times, as well as an increase in the total time required to reach equilibrium. d) The equilibrium swelling ratio (Q_{eq}) for all gel formulations are plotted as a function of cross-linker fraction. All data are for gels swelled in water.

where τ describes the characteristic swelling time; this exponential relationship is commonly used to describe gel swelling [26, 54–58]. The measured τ values (Fig. 2c) decrease with increasing cross-linker fraction, regardless of the cross-linker employed. When PEGDA-700 is employed, the 1:99 formulation experiences a much larger time to reach equilibrium ($\tau \approx 120$ minutes) than the formulations with higher PEGDA-700 content (all $\tau \leq 61$ minutes). Similarly, when PEGDA-10,000 is used as the cross-linker, the 10k 1:99 formulation exhibits

the highest τ value ($\tau \simeq 190$ minutes), and increasing cross-linker fraction lowers τ . Overall, networks with lower cross-linker content imbibe a higher fraction of water (see **Fig. 2d**), and also take more time to reach equilibrium. In other words, when the constraints in the network are increased (via increased cross-linking), the total capacity to swell decreases and therefore less solvent is required to reach equilibrium.

At all cross-linker loadings, the formulations using the PEGDA-10,000 cross-linker have a larger τ , which demonstrates that increasing the length of the cross-linker (PEGDA) corresponds to an increase in the time to reach equilibrium. The increased flexibility afforded by a higher MW cross-linker (PEGDA-10,000) means that the network has more freedom to accommodate solvent during swelling.

3.3 Effect of External Diffusive Pressure on Swelling

The \bar{Q} and τ behavior for swelling PEGDA-700 and PEGDA-10,000 gels in water highlight how the rate of solvent imbibement during swelling is influenced by the internal constraints of the polymer network. This is consistent with the Flory-Rehner (FR) polymer solution thermodynamics model, which postulates that gel swelling is described by an overall osmotic pressure (Π), that is composed of two main terms, the pressure of mixing (Π_{mix}) and the pressure of elasticity (Π_{el}) (see **Eq. 4**) [18, 19, 59–62]. The sum of the pressure of mixing (Π_{mix}) and the pressure of elasticity (Π_{el}) equals the overall osmotic pressure (Π) that the material experiences during swelling. Total osmotic pressure (Π) and mixing pressure (Π_{mix}) are positive values that represent the forces that *drive* swelling, while (Π_{el}) is always negative, representing the *resistance* to swelling that the elasticity of the polymer network asserts.

$$\begin{aligned}\Pi_{mix} &= -\frac{k_B T}{\alpha^3} [\phi + \ln(1 - \phi) + \chi\phi^2] \\ \Pi_{el} &= \frac{k_B T N_c}{V_0} \left[\frac{\phi}{2\phi_0} - \left(\frac{\phi}{\phi_0} \right)^{\frac{1}{3}} \right] \\ \Pi &= \Pi_{mix} + \Pi_{el}\end{aligned}\tag{4}$$

Π_{el} accounts for network constraints through the term N_c , which is a count of all chains within the network [17], and is typically on the order of $10^{18} - 10^{20}$ and increases with cross-link density. When cross-linking increases (e.g., increase in N_c), Π_{el} will become more negative, and there is more resistance to swelling. In other words, increasing cross-linking decreases the freedom chains have to accommodate imbibed solvent.

Table 2: Definition of terms in Flory-Rehner’s theory of osmotic pressure

Term	Definition
k_B	Boltzmann’s constant
α	Effective solvent diameter
ϕ	Volume fraction of polymer
ϕ_0	Initial volume fraction (equals 1 for neat polymer)
χ	Flory-Huggins interaction parameter
N_c	Number of chains in the polymer network
V_0	Initial volume

Π_{mix} represents the driving force for swelling that originates from the attraction between the polymer network and the solvent, which is often characterized by the interaction parameter χ . Π_{mix} also accounts for how the size of a solvent molecule impacts physical mixing. Inspired by the equilibrium FR model, we believe that both the external diffusive pressure during swelling and the elastic network both can be leveraged, even in the transient state, to manipulate the rate of solvent imbibement.

The experiments presented up to this point explicitly manipulate the elastic contribution to swelling (i.e., network constraints). To systematically vary the external diffusive pressure and establish how that impacts instability behaviors, PEGDA-700 samples were swelled in varying (co)solvents comprised of water and ethanol. Initial swelling rates, which were estimated by performing a linear fit to the first 30 minutes of the swelling ratio $Q(t)$, were calculated for all gel formulations with PEGDA-700 as the cross-linker, and are plotted in **Fig. S1**. Overall, swelling in ethanol resulted in a significant decrease in initial swelling rate at all PEGDA-700 fractions. Additionally, for swelling in both water and ethanol, the initial

rate of swelling decreases as cross-linker fraction increases. This data demonstrates how the external diffusive pressure, which can be manipulated via solvent selection, is a means to further manipulate the timescale of swelling.

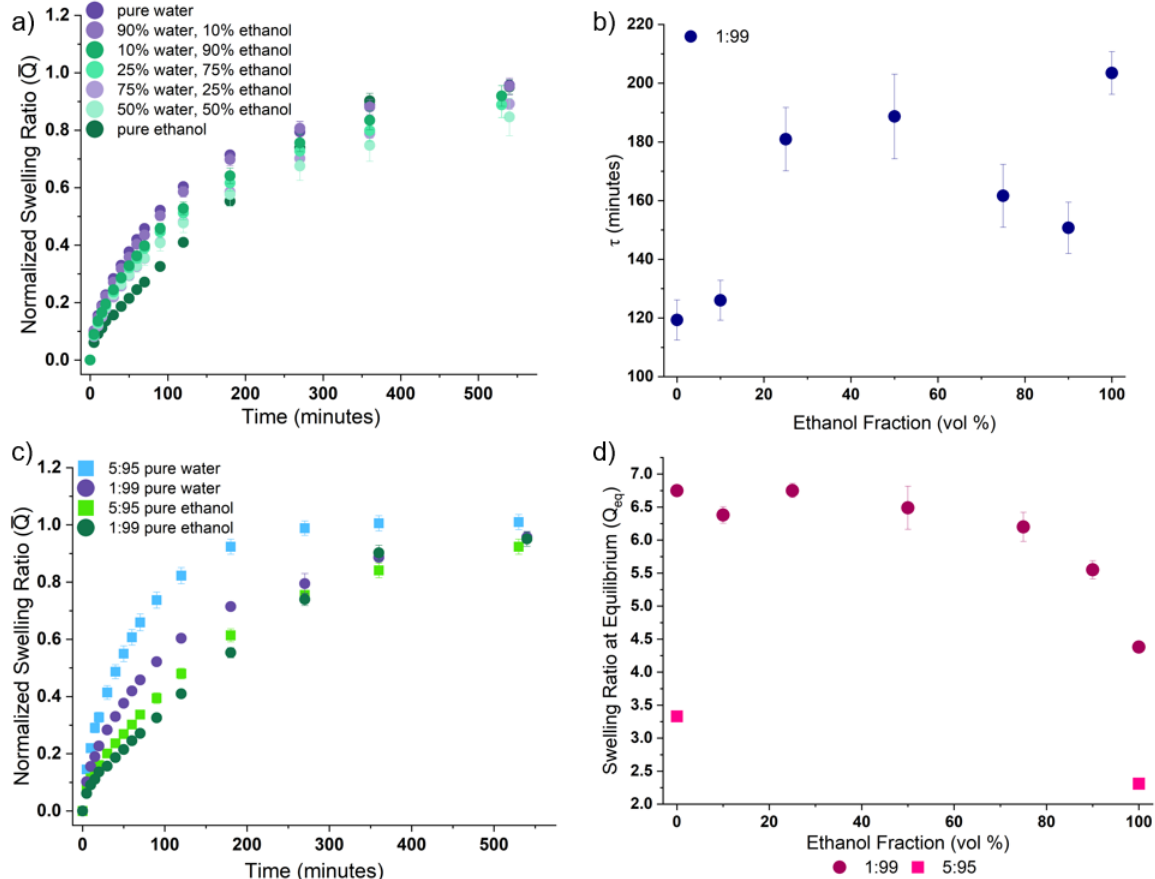


Figure 3: Swelling kinetics for ethanol, water, and ethanol/water (co)solvents. a) Evolution of the normalized swelling ratio (\bar{Q}) for the 1:99, PEGDA-700 formulation in a series of water:ethanol co-solvents. b) The characteristic swelling time, τ , for the 1:99, 700MW formulation for all (co)solvents. c) Comparison of the evolution of the normalized swelling ratio (\bar{Q}) for the 1:99 and 5:95 PEGDA-700 formulations in pure water and pure ethanol. d) Equilibrium swelling ratio (Q_{eq}) for the 1:99, PEGDA-700 formulation for all (co)solvents shows that increasing the amount of ethanol in the (co)solvent generally decreases the Q_{eq} . The Q_{eq} for 5:95, PEGDA-700 formulation in both pure water and pure ethanol are included for reference, and highlight the impact of cross-linker fraction on Q_{eq} .

To better understand the impact of external diffusive pressure, particularly on transient surface instabilities, the PEGDA-700 1:99 formulation was chosen for further analysis. Specifically, \bar{Q} was characterized for the 1:99 formulation when swelling was conducted in pure water, pure ethanol, and 5 co-solvent mixtures (**Fig. 3a**). The solvent-driven changes in \bar{Q} are consistent with the initial swelling rate and are further reflected in the τ parameters

(**Fig. 3b**). To explore the effect of changing network architecture, we measured swelling for two different cross-link densities; 1:99 and 5:95. As shown in **Fig. 2b**, increasing cross-link density leads to faster equilibration times. This may be attributed to the fact that the network imbibes less overall solvent (Q_{eq} , **Fig. 3d**).

Water is known to be a better solvent for these PEG gels, and thus we expect that as the fraction of ethanol in the (co)solvent mixture increases, \overline{Q} will decrease and τ will increase. Surprisingly, we find instead that τ changes non-monotonically with ethanol vol% (**Fig. 3b**). This indicates that there are competing interactions between water and ethanol that interfere with diffusion into the polymer network during swelling in a mixed solvent.

To understand this non-monotonic relationship, we must quantify the attraction between the (co)solvent molecules and the polymer network. The standard method of quantifying interactions is the Flory-Huggins (FH) interaction parameter (χ). χ can be estimated between two species (α and β) using **Eq. 5** [63]:

$$\chi_{\alpha\beta} = \left(\frac{z}{2}\right) \frac{[\epsilon_{\alpha\alpha} + \epsilon_{\beta\beta} - 2\epsilon_{\alpha\beta}]}{k_B T} \quad (5)$$

$$\alpha \equiv A, B, \beta \equiv B, C \neq \alpha$$

Here, z is the coordination number (i.e., the total number of molecules bonded to a central atom), $\epsilon_{\alpha\alpha}$ is the self-attractive energy for species α , $\epsilon_{\beta\beta}$ is the self-attractive energy for species β , and $\epsilon_{\alpha\beta}$ is the interaction energy between species α and β . Positive (+) values of χ indicate that mixing is not energetically favorable, whereas negative (-) values of χ indicate that mixing is favorable. Experimentally determined χ for a ternary mixture of water, ethanol, and linear PEG chains with molecular weights 8650 $\frac{g}{mol}$ and 12600 $\frac{g}{mol}$ are reported in **Table 3** [64]. While these measurements are for linear PEG systems, and may not directly correspond to χ measured for a cross-linked PEG system, they can help us understand how our ternary mixture interacts.

Table 3 shows that mixing of water and PEG is slightly unfavorable, mixing PEG and

Table 3: Experimentally measured Flory-Huggins interaction parameters (χ). χ for the ternary water-PEG-ethanol mixture were determined by Song-Ping Luh for two molecular weights of PEG [64].

Flory-Huggins interaction parameter	PEG 8650	PEG 12600
$\chi_{water-PEG}$	1.0001	0.6318
$\chi_{water-ethanol}$	-4.4412	-4.2339
$\chi_{PEG-ethanol}$	-0.6862	-0.7451

ethanol is favorable, and mixing water and ethanol is significantly favorable (due to the large, negative $\chi_{water-ethanol}$). This can explain the non-monotonic swelling behavior we observe in (co)solvent mixtures: water and ethanol are significantly attracted to one another, meaning the interaction between these solvent species likely competes with the driving force of swelling [63]. The normalized swelling ratio (\bar{Q}) data for swelling in (co)solvent mixtures supports this finding (**Fig. 3a**). The \bar{Q} behavior for 10/90 and 90/10 (vol/vol, water/ethanol) (co)solvents are very similar to pure water behavior (**Fig. 3a**), which is similar to findings from ternary mixtures with linear PEG polymers [63]. More specifically, when (co)solvent species experience significant interaction with each other, the miscibility between the (co)solvent mixture and the polymer network is decreased, and immiscibility reaches its maximum when the volume ratio between the (co)solvent species is equal to one. Indeed, **Fig.3b** shows that the 50/50 (vol/vol) (co)solvent mixture exhibits the highest τ value, indicating that the ternary mixture reaches its peak immiscibility when water and ethanol are mixed in equal parts. This is particularly interesting, as this behavior does not follow established co-non-solvency and co-solvency behaviors in gel swelling [65–67], as our two (co)solvents have differing interactions with the gel (e.g. positive vs. negative χ).

While the χ values for water-PEG and PEG-ethanol indicate better mixing when gels are swollen in ethanol, our data shows reduced Q_{eq} and initial swelling rate in ethanol (**Fig. 3d** and **Fig. S1**, respectively). This can be explained by considering the solvent molecular size. Flory-Rehner theory (see **Eq. 4**) states that the pressure of mixing (Π_{mix}) is inversely proportional to the solvent diameter cubed, meaning that increasing the size of the

solvent molecule would significantly decrease the pressure of mixing (i.e., the driving force for swelling). The effective diameter of a water molecule is 2.75 \AA [68], and the diameter of an ethanol molecule is 4.5 \AA [69]. This is consistent with our experimental observation that the network swells considerably more in water. Although ethanol is a better solvent for *linear* PEG chains, its larger size hinders its ability to mix with the three-dimensional, cross-linked PEG network.

3.4 Examining Surface Creasing during Swelling

Changing the solvent mixture changes the rate of solvent imbibement, and thus impacts transient material stress. To quantify these changes, we studied the evolution of surface instabilities during swelling in water, ethanol, and (co)solvent mixtures. We used light microscopy to image surface instabilities *in situ* and characterize pattern evolution. The surface deformation of the 1:99, PEGDA-700 formulation was characterized during swelling in ethanol, water, and (co)solvent mixtures (**Fig. 4**).

The observed crease evolution in water (**Fig. 4a**, corresponding binary tracings **Fig. 4b**) and in ethanol (**Fig. 4c**, corresponding binary tracings **Fig. 4d**), show that surface deformation began rapidly once the gel was placed in solvent. We note that the images show creasing on both the bottom (in-focus sharp lines) and top of the sample (larger darker out-of-focus lines); Analysis was done on the creases on the bottom of the sample as highlighted in **Fig. S3** and **Fig. S4**. **Fig. 4** shows that swelling in ethanol leads to a higher number of creases when compared to swelling in water. This is quantified in **Fig. 4e**, which shows the mean density of creases as a function of swelling time in the various (co)solvent mixtures. The density of creases rapidly decreases in time. This large, relatively fast decrease is due to relaxation of the outermost layer of the gel as diffusion of the solvent continues deeper into the network. At all time points, swelling in pure ethanol results in significantly more creases than any other (co)solvent, and swelling in pure water shows the lowest number of creases. The three co-solvent mixtures explored fell between these extremes and are statistically

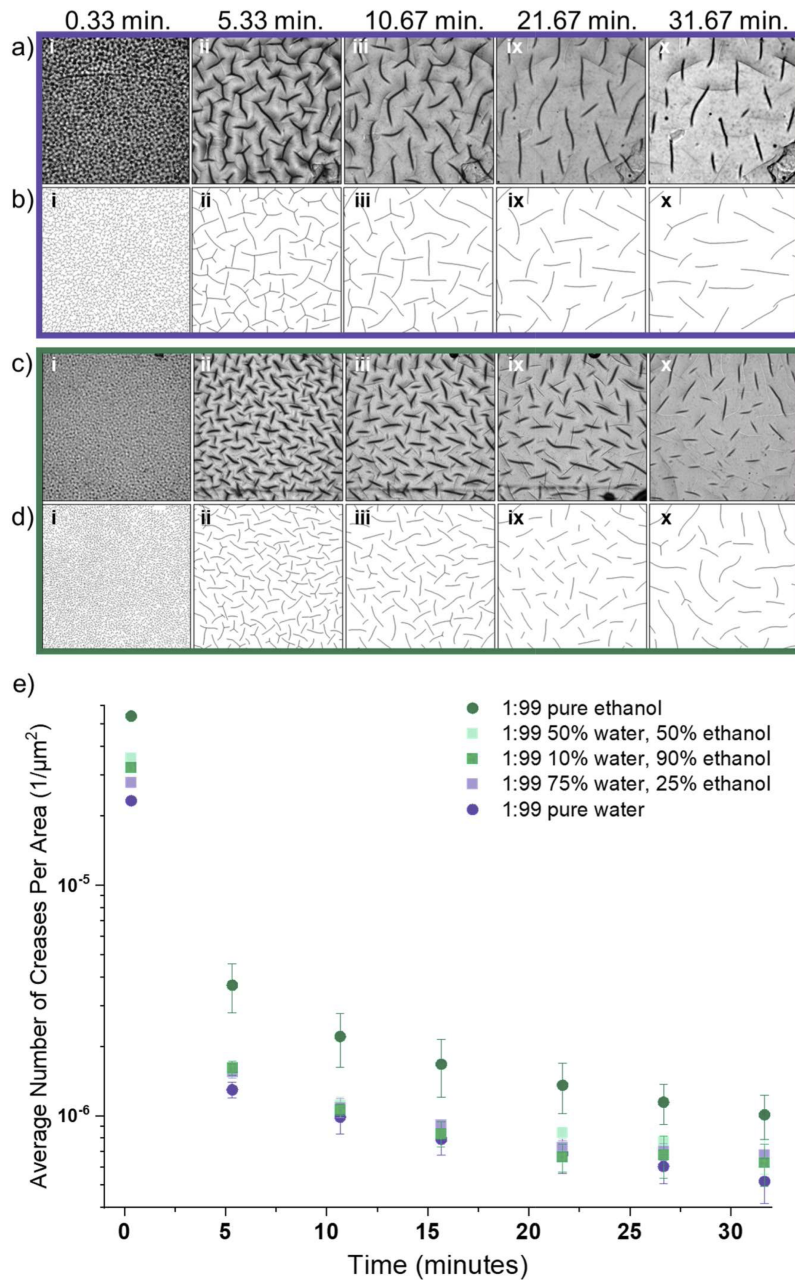


Figure 4: Surface creasing during swelling in water, ethanol, and water-ethanol (co)solvents. **a)** Microscope images taken of a 1:99, PEGDA-700 sample swelling in *water* for i) 0.33, ii) 5.33, iii) 10.67, ix) 21.67, and x) 31.67 minutes. **b)** The creases in each microscope image were manually traced in order to accurately identify and binarize the patterns, **c)** Microscope images of a 1:99, PEGDA-700 sample swelled in *ethanol* for i) 0.33, ii) 5.33, iii) 10.67, ix) 21.67, and x) 31.67 minutes, as well as the **d)** corresponding traced crease patterns. **e)** The average number of creases was measured and divided by the image area for 1:99, PEGDA-700 formulation samples swelled in pure water, pure ethanol, and three (co)solvent mixtures. This analysis reveals there are a large number of creases at the onset of swelling, and a significant decrease in number of creases after five minutes of swelling. The number of creases continue to gradually decrease over 30 minutes of observation.

similar.

As shown in **Fig. S1**, swelling the 1:99 formulation in water significantly increases the initial rate of swelling compared to ethanol. The slower imbibement of ethanol corresponds to a lower driving force for swelling and less mixing pressure (Π_{mix}) forcing the network to relax and dissipate the compressive stress at the surface. Despite the fact that the network imbibes significantly less fluid during swelling in ethanol as compared to water, this results in twice the number of surface creases (**Fig. 4e**). This suggests that (co)solvent selection and the associated diffusivity within a gel network is a significant parameter when tailoring the scale of instabilities that form.

Wrinkling of soft materials under compression is well-characterized, and theories have been developed to connect wrinkling wavelength directly with material properties [36]. The features we observe in this gel system are creases (as opposed to wrinkles), as evidenced by their random orientation. This indicates the material has made self-contact, which presents a challenge for connecting these patterns to network material properties. However, the assumption from classical wrinkling of a skin layer atop a foundation is similar to the initial states of swelling when just a thin, outermost layer of the gel has imbibed solvent. Wrinkling theory predicts that the compressive force at the surface is related to the skin thickness, the elastic modulus and Poisson’s ratio of both the skin and the bulk [36]. As the compressive force increases, the wavelength of wrinkles decreases. Thus, the lower number of features (**Fig.4e**), and the higher spacing (i.e., “wavelength”) we observe when swelling in water likely represents lower compressive forces at the surface, particularly at early time points.

To quantify crease spacing, we measure the mean inter-crease distance for each solvent condition (**Fig. 5a**). This analysis shows that the average crease spacing at all times is lowest for ethanol, indicating higher compressive stress. As time evolves, the crease distance rapidly increases, which correlates to a relaxation of the polymer network with time. Similar to the average number of creases, all solvent conditions show a dramatic increase in the distance between creases between 0.33 min. and 5.33 min. (i.e., between a 300% and a 400%

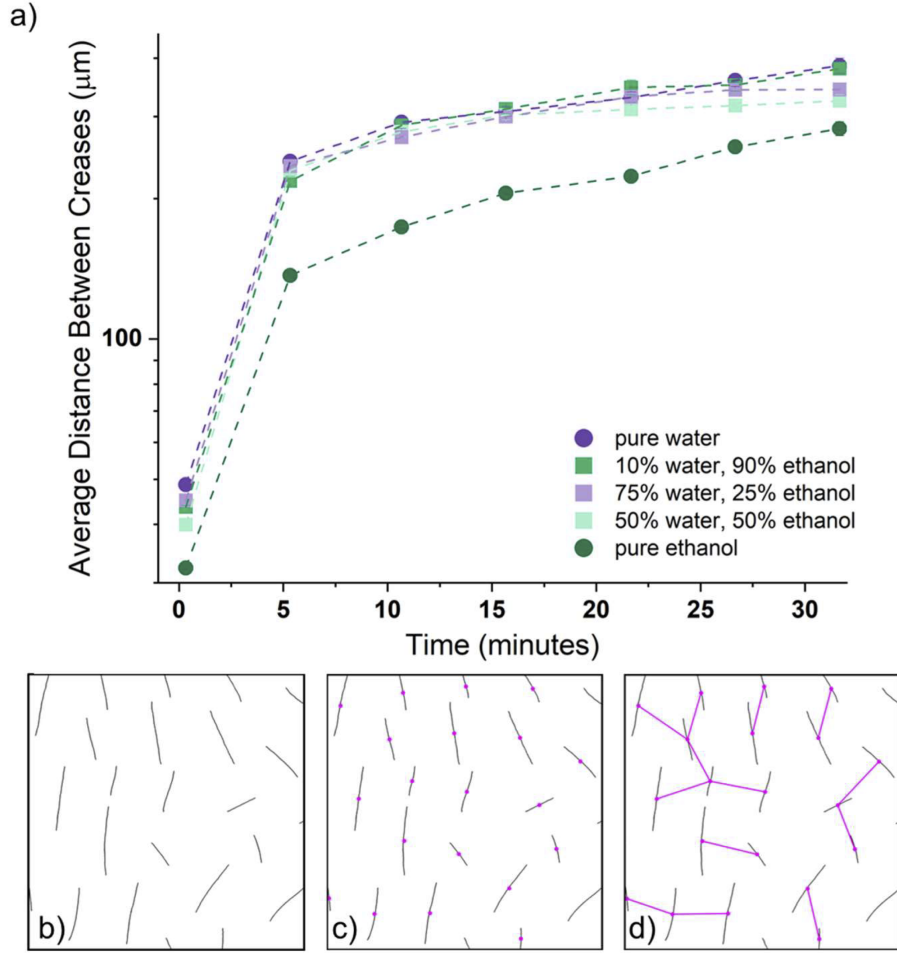


Figure 5: Characteristic distance between creases. a) Analysis of the traced crease patterns was performed to determine the average distance between creases for the 1:99, PEGDA-700 formulation swelled in pure water, pure ethanol, and three (co)solvent mixtures. At all times, the distance between creases in pure ethanol is smaller than the other conditions. b) Example tracing of swelling in water to demonstrate how the average distance was determined. First, each individual crease was identified, c) followed by calculation of the geometric mean, and a location was assigned for each crease (indicated by purple dots). d) For each crease, the closest neighbor was identified, and the distance between them was measured. This process was repeated for each crease, and any repeated distances (i.e., a pair of creases that reported one another as their nearest neighbor with the same distance value) were eliminated. (a) reports the mean distance across the triplicate samples for each solvent condition.

increase). This increase in distance between creases (our analogue to wavelength) indicates a decrease in compressive stress at the surface due to the immediate relaxation that occurs at the surface of the gel.

Interestingly, at late times, the 50/50 water/ethanol (co)solvent plateaued and diverged slightly from the grouping of the pure water and other (co)solvent mixtures. A similar trend appeared in the number of creases (**Fig. 4a**). This result can be understood in the context

of the (co)solvent theory that immiscibility is greatest when the ratio $\frac{\phi_{ethanol}}{\phi_{water}}$ is equal to 1. The interaction between water and ethanol that competes with swelling is greatest when the (co)solvent contains equal parts of water and ethanol. This significant interference leads to the (co)solvent mixture behaving as a worse solvent.

4 Conclusions

We explore the impact of internal network constraints (cross-linking) and external diffusive pressure (solvent quality) on swelling kinetics and surface deformation dynamics in PEG-based gels. We find that networks with fewer internal constraints (which have a higher overall capacity for swelling, Q_{eq}), experience much longer transient swelling. Increasing the molecular weight between cross-links decreases the elastic pressure, and thus increases the time it takes to reach equilibrium. We find that ethanol, despite having a large negative χ , is a worse solvent for the network than water. This demonstrates that while imbibement is a function of chemical affinity (χ), this competes with the effect of molecular size. Swelling experiments in water-ethanol (co)solvent mixtures reveal that the strong affinity between water and ethanol competes with the driving force of swelling.

Measurements of surface instabilities show that immediately after being placed in a solvent, densely packed creases rapidly appear on the surface of the gel. The inter-crease spacing increases in time as diffusion progresses and the material begins to relax. Furthermore, we find that swelling in ethanol results in a higher crease density, which likely indicates that larger compressive stresses are present. Thus, swelling in ethanol not only slows down swelling kinetics, but it also alters the dynamics of surface deformations. This reveals that the driving force for mixing is lower for swelling in ethanol as compared to water, and therefore the hydrogel network experiences less pressure to relax and dissipate the stress that builds due to swelling and solvent diffusion. The physics involved in generating macroscopic surface deformations is complex, and thus it is challenging to use the geometry of these features to directly quantify material stresses. However, this work establishes a path towards understanding the complex dynamics at play during transient swelling and offers a new way to quantify material response.

Acknowledgements

During this study, Alyssa VanZanten was fully supported and Shih-Yuan Chen was partially supported by NSF Grant DMR 2311697. The authors would like to thank our labmates Sabrina Curley, Denghao Fu, and Samira Kahn, for their support and rigorous discussion.

References

- [1] Bingwei Xin and Jingcheng Hao. Reversibly switchable wettability. *Chemical Society Reviews*, 39:769–782, 1 2010.
- [2] Songshan Zeng, Rui Li, Stephan G. Freire, Vivian M.M. Garbellotto, Emily Y. Huang, Andrew T. Smith, Cong Hu, William R.T. Tait, Zichao Bian, Guoan Zheng, Dianyun Zhang, and Luyi Sun. Moisture-responsive wrinkling surfaces with tunable dynamics. *Advanced Materials*, 29:1700828, 6 2017.
- [3] Yu Huang, Birgitt Boschitsch Stogin, Nan Sun, Jing Wang, Shikuan Yang, and Tak Sing Wong. A switchable cross-species liquid repellent surface. *Advanced Materials*, 29:1604641, 2 2017.
- [4] Theodore Manouras and Maria Vamvakaki. Field responsive materials: Photo-, electro-, magnetic- and ultrasound-sensitive polymers. *Polymer Chemistry*, 8:74–96, 1 2017.
- [5] Zhen Jiang, Ming Li Tan, Mahdiar Taheri, Qiao Yan, Takuya Tsuzuki, Michael G. Gardiner, Broden Diggle, and Luke A. Connal. Strong, self-healable, and recyclable visible-light-responsive hydrogel actuators. *Angewandte Chemie International Edition*, 59(18):7049–7056, 2020.
- [6] Xiao-Qiao Wang, Shengyang Yang, Cai-Feng Wang, Li Chen, and Su Chen. Multifunctional hydrogels with temperature, ion, and magnetocaloric stimuli-responsive performances. *Macromolecular Rapid Communications*, 37(9):759–768, 2016.
- [7] Christopher S Brazel and Nikolaos A Peppas. Mechanisms of solute and drug transport in relaxing, swellable, hydrophilic glassy polymers. *Polymer*, 1998.
- [8] Paolo Colombo, Ruggero Bettini, Gina Massimo, Pier Luigi Catellani, Patrizia Santi, and Nikolaos A. Peppas. Drug diffusion front movement is important in drug release control from swellable matrix tablets. *Journal of Pharmaceutical Sciences*, pages 47907–1283, 1994.
- [9] Ross Devolder and Hyun Joon Kong. Hydrogels for in vivo-like three-dimensional cellular studies. *Wiley Interdisciplinary Reviews: Systems Biology and Medicine*, 4:351–365, 7 2012.
- [10] Ankit Gargava, Chandamany Arya, and Srinivasa R. Raghavan. Smart hydrogel-based valves inspired by the stomata in plants. *ACS Applied Materials and Interfaces*, 8:18430–18438, 7 2016.
- [11] Mohammad Saidi, Alaleh Dabbaghi, and Sohrab Rahmani. Swelling and drug delivery kinetics of click-synthesized hydrogels based on various combinations of peg and star-shaped pcl: influence of network parameters on swelling and release behavior. *Polymer Bulletin*, 77:3989–2010, 2020.

- [12] Hajime Tanaka, Hidemi Tomita, Atsunori Takasu, Takafumi Hayashi, and Toshio Nishi. Morphological and kinetic evolution of surface patterns in gels during the swelling process: Evidence of dynamic pattern ordering. *The American Physical Society*, 68:2794–2797, 1992.
- [13] Riku Takahashi, Yumihiko Ikura, Daniel R. King, Takayuki Nonoyama, Tasuku Nakajima, Takayuki Kurokawa, Hirotooshi Kuroda, Yoshihiro Tonegawa, and Jian Ping Gong. Coupled instabilities of surface crease and bulk bending during fast free swelling of hydrogels. *Soft Matter*, 12:5081–5088, 2016.
- [14] François Weiss, Shengqiang Cai, Yuhang Hu, Min Kyoo Kang, Rui Huang, and Zhigang Suo. Creases and wrinkles on the surface of a swollen gel. *Journal of Applied Physics*, 114:073507, 8 2013.
- [15] Jungwook Kim. Morphological analysis of crease patterns formed on surface-attached hydrogel with a gradient in thickness. *Journal of Applied Polymer Science*, 131, 7 2014.
- [16] Paul J. Flory and John Rehner. Statistical mechanics of cross-linked polymer networks i. rubberlike elasticity. *The Journal of Chemical Physics*, 11:512–520, 1943.
- [17] Paul J. Flory and John Rehner. Statistical mechanics of cross-linked polymer networks ii. swelling. *The Journal of Chemical Physics*, 11:521–526, 1943.
- [18] Jean-François Louf, Nancy B Lu, Margaret G O’connell, H Jeremy Cho, and Sujit S Datta. Under pressure: Hydrogel swelling in a granular medium. *Sci. Adv*, 7:11, 2021.
- [19] Manuel Quesada-Pérez, José Alberto Maroto-Centeno, Jacqueline Forcada, and Roque Hidalgo-Alvarez. Gel swelling theories: The classical formalism and recent approaches. *Soft Matter*, 7:10536–10547, 11 2011.
- [20] Fernando T. P. Borges, Georgia Papavasiliou, and Fouad Teymour. Characterizing the molecular architecture of hydrogels and crosslinked polymer networks beyond flory–rehner—i. theory. *Biomacromolecules*, 21(12):5104–5118, 2020. PMID: 33253542.
- [21] Fernando T. P. Borges, Georgia Papavasiliou, and Fouad Teymour. Characterizing the molecular architecture of hydrogels and crosslinked polymer networks beyond flory–rehner. ii: Experiments. *Biomacromolecules*, 24(4):1585–1603, 2023. PMID: 36929746.
- [22] Kelsey-Ann Leslie, Robert Doane-Solomon, Srishti Arora, Sabrina J. Curley, Caroline Szczepanski, and Michelle M. Driscoll. Gel rupture during dynamic swelling. *Soft Matter*, 2021.
- [23] Nikolaos A Peppas and Edward W Merrill. Crosslinked poly(vinyl alcohol) hydrogels as swollen elastic networks. *JOURNAL OF APPLIED POLYMER SCIENCE*, 21:1763–1770, 1977.

- [24] Melle T.J.J.M. Punter, Hans M. Wyss, and Bela M. Mulder. Compression and swelling of hydrogels in polymer solutions: A dominant-mode model. *Physical Review E*, 102:062607, 12 2020.
- [25] M. Jesús Molina, M. Rosa Gómez-Antón, and Inés F. Piérola. Determination of the parameters controlling swelling of chemically cross-linked ph-sensitive poly(n-vinylimidazole) hydrogels. *Journal of Physical Chemistry B*, 111:12066–12074, 10 2007.
- [26] Yong Li and Toyochi Tanaka. Kinetics of swelling and shrinking of gels. *The Journal of Chemical Physics*, 92:1365–1371, 1990.
- [27] A.D. Drozdov, A.A. Papadimitriou, J.H.M. Liely, and C.-G. Sanporean. Constitutive equations for the kinetics of swelling hydrogels. *Mechanics of Materials*, 102:61–73, 2016.
- [28] J. Jr. Rehner. Polymer solvent interaction parameter. *Polymer Science and Technology*, 9, 1975.
- [29] Toyochi Tanaka and David J. Fillmore. Kinetics of swelling of gels. *The Journal of Chemical Physics*, 70:1214–1218, 1979.
- [30] Shawn A. Chester. A constitutive model for coupled fluid permeation and large viscoelastic deformation in polymeric gels. *Soft Matter*, 8:8223–8233, 8 2012.
- [31] Abigail Plummer, Caroline Adkins, Jean-François Louf, Andrej Košmrlj, and Sujit S. Datta. Obstructed swelling and fracture of hydrogels. *Soft Matter*, 7 2023.
- [32] Michele Curatolo, Paola Nardinocchi, Eric Puntel, and Luciano Teresi. Transient instabilities in the swelling dynamics of a hydrogel sphere. *Journal of Applied Physics*, 122:145109, 10 2017.
- [33] Jingyi Guo, Alan T. Zehnder, Costantino Creton, and Chung Yuen Hui. Time dependent fracture of soft materials: linear versus nonlinear viscoelasticity. *Soft Matter*, 16:6163–6179, 7 2020.
- [34] Md Rashedul Islam, Sheik Tanveer, and Chau Chyun Chen. Modeling swelling behavior of hydrogels in aqueous organic solvents. *Chemical Engineering Science*, 242:116744, 10 2021.
- [35] Pengfei Yang, Yaopeng Fang, Yanan Yuan, Shun Meng, Zihao Nan, Hui Xu, Haroon Imtiaz, Bin Liu, and Huajian Gao. A perturbation force based approach to creasing instability in soft materials under general loading conditions. *Journal of the Mechanics and Physics of Solids*, 151:104401, 6 2021.
- [36] Jan Genzer and Jan Groenewold. Soft matter with hard skin: From skin wrinkles to templating and material characterization. *Soft Matter*, 2:310–323, 2006.
- [37] Shu Yang, Krishnacharya Khare, and Pei Chun Lin. Harnessing surface wrinkle patterns in soft matter. *Advanced Functional Materials*, 20:2550–2564, 8 2010.

- [38] E. Cerda and L. Mahadevan. Geometry and physics of wrinkling. *Physical Review Letters*, 90:4, 2003.
- [39] Verónica Trujillo, Jungwook Kim, and Ryan C. Hayward. Creasing instability of surface-attached hydrogels. *Soft Matter*, 4:564–569, 2008.
- [40] Jianzhu Ju, Ken Sekimoto, Luca Cipelletti, Costantino Creton, and Tetsuharu Narita. Heterogeneous nucleation of creases in swelling polymer gels. *Physical Review E*, 105:034504, 3 2022.
- [41] Bin Xu and Ryan C. Hayward. Low-voltage switching of crease patterns on hydrogel surfaces. *Advanced Materials*, 25:5555–5559, 10 2013.
- [42] Samuel James Dupont, Ryan Scott Cates, Peter George Stroot, and Ryan Toomey. Swelling-induced instabilities in microscale, surface-confined poly(n-isopropylacrylamide) hydrogels. *Soft Matter*, 6:3876–3882, 8 2010.
- [43] William Toh, Zhiwei Ding, Teng Yong Ng, and Zishun Liu. Wrinkling of a polymeric gel during transient swelling. *Journal of Applied Mechanics, Transactions ASME*, 82:061004, 6 2015.
- [44] Murat Guvendiren, Shu Yang, and Jason A. Burdick. Swelling-induced surface patterns in hydrogels with gradient crosslinking density. *Advanced Functional Materials*, 19:3038–3045, 10 2009.
- [45] Jianjun Gu, Xiaoyun Li, Hancheng Ma, Ying Guan, and Yongjun Zhang. One-step synthesis of phema hydrogel films capable of generating highly ordered wrinkling patterns. *Polymer*, 110:114–123, 2017.
- [46] Murat Guvendiren, Jason A. Burdick, and Shu Yang. Kinetic study of swelling-induced surface pattern formation and ordering in hydrogel films with depth-wise crosslinking gradient. *Soft Matter*, 6:2044–2049, 2010.
- [47] Juan Rodríguez-Hernández. Wrinkled interfaces: Taking advantage of surface instabilities to pattern polymer surfaces. *Progress in Polymer Science*, 42:1–41, 2015.
- [48] Hans Scholt. Kinetics of swelling of polymers and their gels first-order swelling kinetics. *American Pharmaceutical Association Journal of Pharmaceutical Sciences I*, 407:467–70, 1992.
- [49] Arne Ilseng, Victorien Prot, Bjørn H. Skallerud, and Bjørn T. Stokke. Buckling initiation in layered hydrogels during transient swelling. *Journal of the Mechanics and Physics of Solids*, 128:219–238, 7 2019.
- [50] Nicolas Zalachas, Shengqiang Cai, Zhigang Suo, and Yuri Lapusta. Crease in a ring of a ph-sensitive hydrogel swelling under constraint. *International Journal of Solids and Structures*, 50:920–927, 3 2013.

- [51] Yuka Kashiwara, Taka Aki Asoh, and Hiroshi Uyama. Travelling wave generation of wrinkles on the hydrogel surfaces. *Macromolecular Rapid Communications*, 43:2100848, 4 2022.
- [52] Zi Liang Wu, Michael Moshe, Jesse Greener, Heloise Therien-Aubin, Zhihong Nie, Eran Sharon, and Eugenia Kumacheva. Three-dimensional shape transformations of hydrogel sheets induced by small-scale modulation of internal stresses. *Nature Communications*, 4:1586, 2013.
- [53] Udaka K. De Silva and Yakov Lapitsky. Preparation and timed release properties of self-rupturing gels. *ACS Applied Materials and Interfaces*, 8:29015–29024, 10 2016.
- [54] A R Berens and H B Hopfenberg. Diffusion and relaxation in glassy polymer powders: 2. separation of diffusion and relaxation parameters, 1978.
- [55] Katherine Zhang, Wuxiang Feng, and Congrui Jin. Protocol efficiently measuring the swelling rate of hydrogels. *MethodsX*, 7:100779, 1 2020.
- [56] Jan Sievers, Karsten Sperlich, Thomas Stahnke, Christine Kreiner, Thomas Eickner, Heiner Martin, Rudolf F. Guthoff, Melanie Schünemann, Sebastian Bohn, and Oliver Stachs. Determination of hydrogel swelling factors by two established and a novel non-contact continuous method. *Journal of Applied Polymer Science*, 138:50326, 5 2021.
- [57] Fariba Ganji, Samira Vasheghani Farahani, Ebrahim Vasheghani-Farahani, and Samira Vasheghani-Farahani. Theoretical description of hydrogel swelling: A review, 2010.
- [58] Daniel M. Gruber, Mark S. Ferris, and Gary Zabow. Real-time in-situ measurement of hydrogel swelling by single sided nmr. *Polymer*, 281:126108, 7 2023.
- [59] Paul J. Flory. *Principles of polymer chemistry*. Cornell University Press, 1953.
- [60] Takamasa Sakai. *Physics of Polymer Gels*. John Wiley and Sons Ltd, 2020.
- [61] S. Hirotsu. Static and time-dependent properties of polymer gels around the volume phase transition. *Phase Transitions*, 47:183–240, 3 1994.
- [62] Michael Rubinstein and Ralph Colby. *Polymer Physics*. Oxford University Press, 2003.
- [63] Jacek Dudowicz, Karl F. Freed, and Jack F. Douglas. Communication: Cosolvency and cononsolvency explained in terms of a flory-huggins type theory. *Journal of Chemical Physics*, 143:131101, 10 2015.
- [64] Song Ping Luh. The cloud point composition and flory-huggins interaction parameters of polyethylene glycol and sodium lignin sulfonate in water-ethanol mixtures redacted for privacy. 1988.
- [65] Debashish Mukherji, Carlos M Marques, and Kurt Kremer. Collapse in two good solvents, swelling in two poor solvents: defying the laws of polymer solubility? *Journal of Physics: Condensed Matter*, 30(2):024002, January 2018.

- [66] Yuji Higaki, Takumi Masuda, Mai Nakamura, and Masaya Takahashi. Cononsolvency-Induced Microphase Separation of Double Hydrophilic Poly(2-ethyl-2-oxazoline)–Polycarboxybetaine Diblock Copolymers in Water–Ethanol Mixtures. *Macromolecules*, 56(16):6208–6216, August 2023.
- [67] Lea Steinbeck, Hanna J. M. Wolff, Maximilian Middeldorf, John Linkhorst, and Matthias Wessling. Porous Anisometric PNIPAM Microgels: Tailored Porous Structure and Thermal Response. *Macromolecular Rapid Communications*, 45(11):2300680, June 2024.
- [68] Paul Schatzberg. On the molecular diameter of water from solubility and diffusion measurements. *The Journal of Physical Chemistry*, pages 4569–4570, 1967.
- [69] Zhuonan Song, Yi Huang, Weiwei L. Xu, Lei Wang, Yu Bao, Shiguang Li, and Miao Yu. Continuously adjustable, molecular-sieving ”gate” on 5a zeolite for distinguishing small organic molecules by size. *Scientific Reports*, 5:13981, 9 2015.

Supporting Information

Table 1: Swelling ratio at equilibrium. The average swelling ratio at equilibrium for all hydrogel formulations and solvent conditions.

Formulation	Solvent	Swelling Ratio at Equilibrium
1:99	Water	6.75
5:95	Water	3.33
10:90	Water	2.67
20:80	Water	2.19
40:60	Water	1.88
10k 1:99	Water	8.85
10k 10:90	Water	4.85
10k 20:80	Water	4.64
10k 40:60	Water	4.42
1:99	Ethanol	4.38
5:95	Ethanol	2.31
10:90	Ethanol	2.13
20:80	Ethanol	1.77
40:60	Ethanol	1.79
1:99	90% water, 10% ethanol	6.38
1:99	75% water, 25% ethanol	6.75
1:99	50% water, 50% ethanol	6.49
1:99	25% water, 75% ethanol	6.20
1:99	10% water, 90% ethanol	5.55

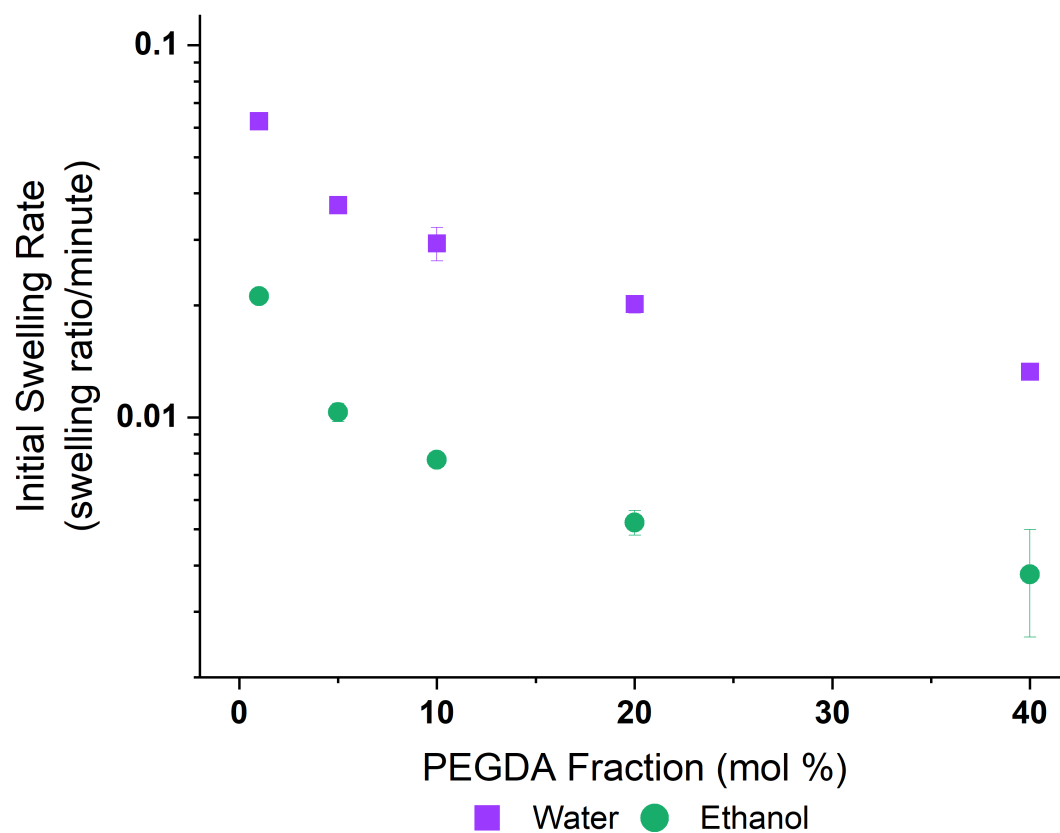


Figure 1: The initial rate of swelling in water (squares) and ethanol (circles) for gel formulations with the 700MW PEGDA cross-linker are compared. The initial rate was measured over the first 30 minutes of swelling. This time period captures the complete evolution of observed creasing instabilities.

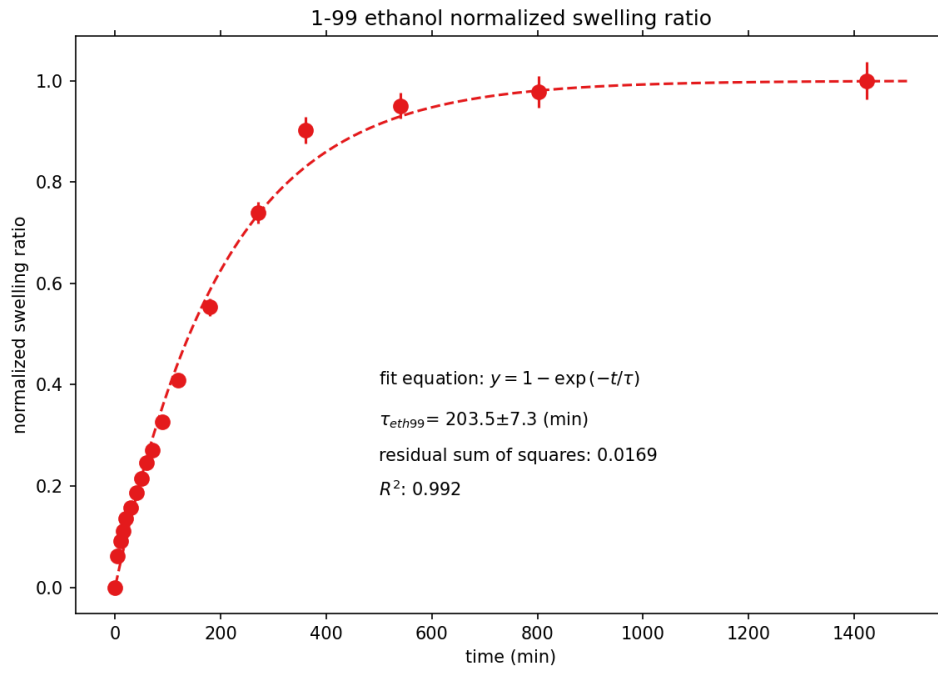


Figure 2: Example of fitting performed to extract τ , the characteristic time to equilibrium. The normalized swelling ratio, \bar{Q} , is plotted and fit with an exponential equation, shown inset in this figure. This fitting output the denominator of the exponential as τ , which describes the time the system, in this case 1:99, PEGDA-700 swelling in ethanol, takes to reach 64% of the total swelling capacity.

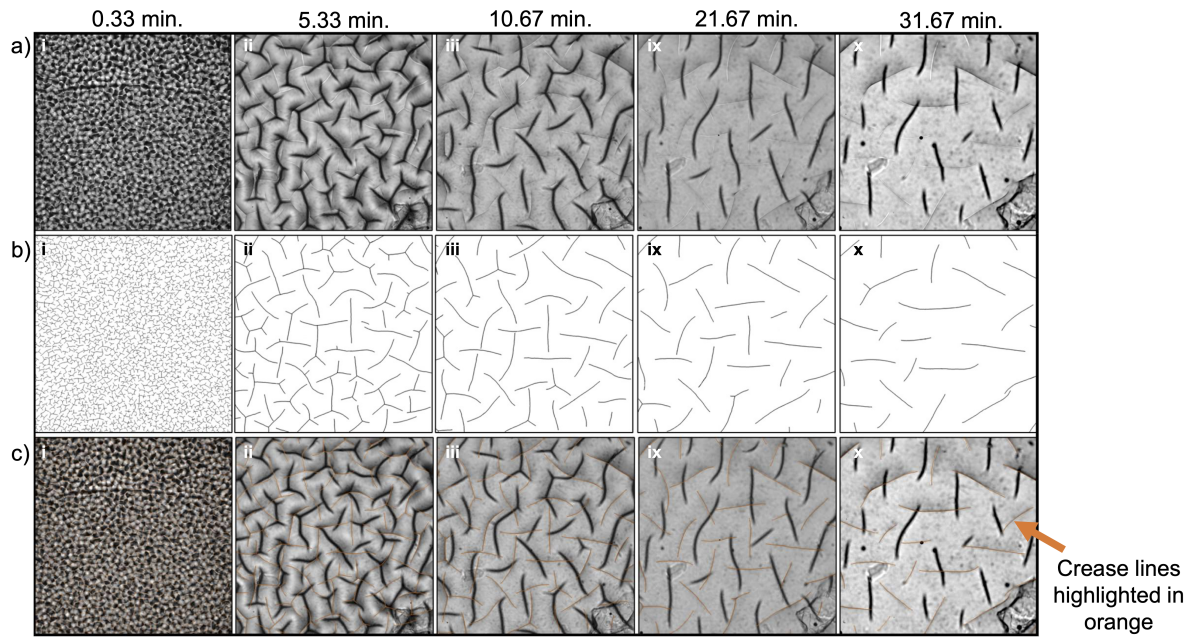


Figure 3: Illustrating crease lines on in-focus surface during swelling in water. a) The microscope images and b) crease tracings shown in **Fig.4** are repeated here. c) The traced crease lines in orange are then overlaid on top of the corresponding microscope images to highlight the location of the deformation features of interest.

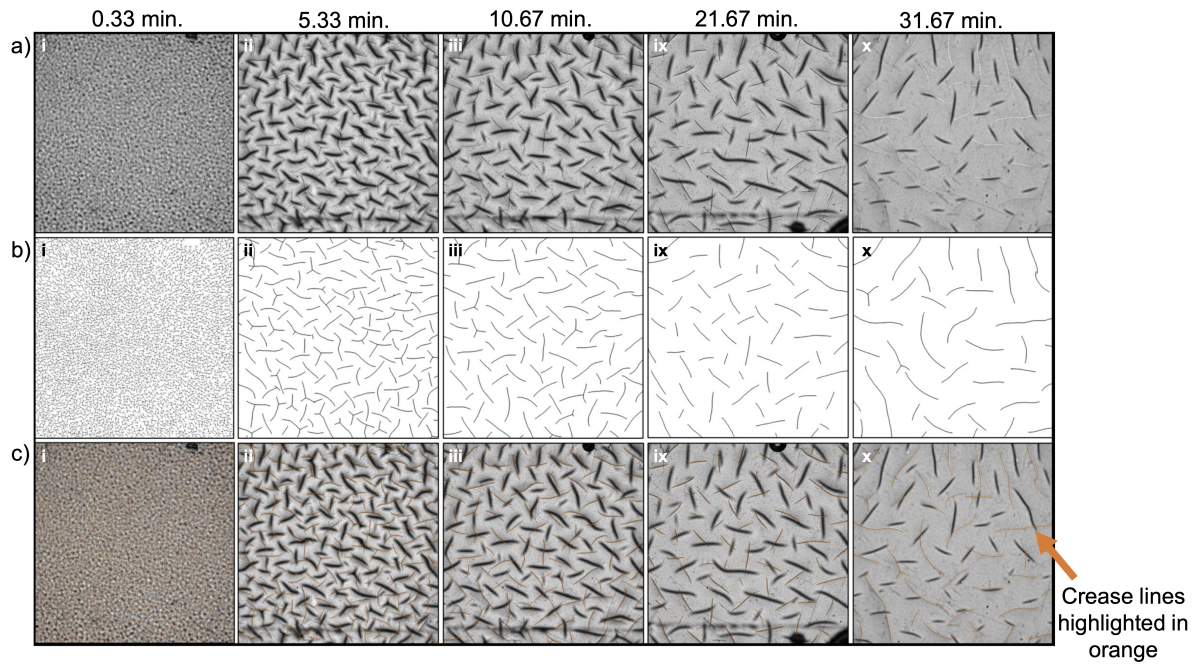


Figure 4: Illustrating crease lines on in-focus surface during swelling in ethanol. a) The microscope images and b) crease tracings shown in **Fig.4** are repeated here. c) The traced crease lines in orange are then overlaid on top of the corresponding microscope images to highlight the location of the deformation features of interest.